JEM Journal of Experimental Medicine

ARTICLE

Nasal germinal centers and IgA class-switch recombination depend on CCR6 and B cell receptor affinity

Jingjing Liu[1], Liat Stoler-Barak[1], and Ziv Shulman[1]

Antibody-mediated immune responses in mucosal tissues are critical for defending against pathogens while maintaining homeostasis with commensals. Nasal vaccination aims to induce local protection in the upper airway mucosa. Although B cell–driven immunity is well characterized in gut-associated lymphoid tissues such as Peyer's patches and mesenteric LNs, much less is known about analogous processes in the upper airways. Here, we show that B cell receptor (BCR) affinity and CCR6 regulate germinal center (GC) seeding and class-switch recombination (CSR) to IgA in nasal-associated lymphoid tissue (NALT) following nasal vaccination. B cells bearing low-affinity BCRs failed to upregulate CCR6 and did not support T follicular helper cell differentiation or seed GCs in the NALT. CCR6-deficient B cells were unable to migrate to the NALT subepithelial dome or undergo IgA CSR and seed GC effectively in response to nasal vaccination or commensal bacteria signals. Thus, effective targeting of B cell clones to induce CCR6 expression is essential for nasal vaccine design.

Introduction

Mucosal surfaces are constantly exposed to commensal bacteria and harmful pathogens (Pizzolla et al., 2017; Moseman et al., 2020). To prevent bacterial invasion into the host tissues, immune cells reside beneath the lamina propria, which is located just under the gut epithelial barrier (Agace and McCoy, 2017). These populations comprise cells of the adaptive immune response, such as various types of T cells, including γδ T cells and Th17, as well as antibody-secreting cells, which help prevent microbes from invading host tissues (Pabst and Slack, 2020; Pabst and Nowosad, 2023; Bemark et al., 2024; Linehan et al., 2015). The mucosal plasma cells originate in the mucosa-associated lymphoid tissues, where B cells encounter antigens and form germinal centers (GCs) (Liu and Shulman, 2022; Mora and von Andrian, 2008; Fritz et al., 2011). IgA is the major immunoglobulin isotype that protects mucosal tissues in mice, and these antibodies can be transported through the gut epithelial lining into the lumen (Siniscalco et al., 2024).

In mice, B cell class switching to IgA mainly occurs in Peyer's patches (PPs), specialized lymphoid organs that lack defined afferent lymphatic vessels, and instead, actively collect antigens from the gut lumen (Lycke and Bemark, 2012). In these lymphoid organs, microfold cells (M cells) in the follicular-associated epithelium (FAE) deliver antigens into the subepithelial dome (SED), a structure not found in typical draining LNs (Schulz and Pabst, 2013; Komban et al., 2019; Kelsall and Strober, 1996; Neutra et al., 1996; Ualiyeva et al., 2024; Cook et al., 2000). In the SED, B cells interact with gut-derived antigens and express CCR6, which attracts them to CCL20, expressed by epithelial cells that cover the PPs, enabling the B cells to respond to local signals (Reboldi and Cyster, 2016; Biram et al., 2019; Bergqvist et al., 2012; Cook et al., 2000). Various cell types that reside in the SED, including dendritic cells and innate-like lymphoid cells, promote class-switch recombination (CSR) to IgA via TGFβ signaling (Reboldi et al., 2016). B cells subsequently modulate the expression of chemoattractant and repellent receptors to support their movement to the mid-follicle area and seed GCs (Green and Cyster, 2012; Gallman et al., 2021; Pereira et al., 2009). Although CCR6 is essential for IgA CSR, CCR6 is not necessary for commensal bacteria-driven GC formation in PPs (Biram et al., 2019; Reboldi et al., 2016; Reimer et al., 2017). Within the PP SED, B cells are subjected to an affinity-based checkpoint, and while low-affinity clones can expand in response to antigen, they cannot progress and seed GCs as their high-affinity counterparts (Biram et al., 2019). In addition to B cells, other cell types are found in the SED, including macrophages and lysozyme-expressing dendritic cells (Bonnardel et al., 2015; Da Silva et al., 2017; Mörbe et al., 2021; Jain et al., 2023), as well as T follicular helper (Tfh) cells that support local cell differentiation (Biram et al., 2019).

In mice, the nasal-associated lymphoid tissue (NALT) also contains the SED microanatomical site, and limited evidence

[1]Department of Systems Immunology, Weizmann Institute of Science, Rehovot, Israel.

Correspondence to Ziv Shulman: ziv.shulman@weizmann.ac.il; Jingjing Liu: jingjing.liu@weizmann.ac.il.

supports the existence of SED features such as M cells in the FAE of additional lymphoid organs, such as the bronchus-associated lymphoid tissue (Kiyono and Fukuyama, 2004; Nacer et al., 2014; Kimura et al., 2019). The NALT hosts chronic GCs that form in response to commensal bacteria under homeostatic conditions (Liu et al., 2024; Randall, 2015). In addition, immune cells within this organ respond to airborne pathogens and nasal vaccines (Liu et al., 2024; Mao et al., 2022). GC B cells in NALT produce antibody-secreting cells that migrate to the nasal tissues, including the turbinate area and the olfactory epithelium, where they secrete IgA antibodies (Wellford et al., 2022; Liu et al., 2024; Nakashima and Hamashima, 1980). This immune cell site is important for the response to airborne pathogens since antibodies are unable to reach the olfactory mucosa; instead, plasma cells enter both this site and the turbinate region and secrete antibodies to provide local protection (Wellford et al., 2022; Gailleton et al., 2025; Liu et al., 2024).

While the roles of B cell translocation to the SED and BCR affinity in PPs are well established, it remains unknown whether they serve a similar function in the NALT. Several recent important studies examined the immune cell composition, including IgA$^+$ B cells, in adenoids of the human upper airways, setting the stage for functional analyses (Coates et al., 2025; Ramirez et al., 2024). Here, we find that low-affinity B cell clones are unable to respond to antigen in the NALT, nor upregulate CCR6. Furthermore, we find that CCR6 is required for IgA formation in the NALT and for effective GC seeding in response to nasal vaccination, but not in response to commensal bacteria. Collectively, this study highlights both shared and unique functions of BCR affinity and CCR6 in B cells within different mucosal non-draining lymph nodes (LNs), which can be leveraged for nasal vaccine design (Lund and Randall, 2021; Hartwell et al., 2022).

Results

B cells carrying low-affinity BCR are unable to seed GCs in the NALT

To study the B cell immune response in the NALT, we used an adoptive cell transfer model with antigen-specific T and B cells followed by nasal vaccination (Liu et al., 2024; Bergqvist et al., 2012). Host mice were adoptively transferred with B1-8^{hi} or B1-8^{lo} B cells (enriched for antigen-specific λ$^+$ cells) that respond to 4-hydroxy-3-nitrophenylacetyl (NP) and CD4$^+$ OT-II T cells specific for an OVA peptide in the context of MHC-II I-Ab (Shulman et al., 2014). The mice were vaccinated i.n. with NP-OVA mixed with the synthetic TLR-4 ligand, monophosphoryl lipid A (MPLA), as an adjuvant (Liu et al., 2024). We did not use LPS as an adjuvant because a previous study showed that it has an adverse effect on GC responses (Biram et al., 2022). After 5 days, the NALTs were dissected and analyzed by either whole-organ imaging using two-photon laser scanning microscopy (TPLSM) or flow cytometry (Fig. 1 A).

To examine the role of BCR affinity in GC formation within the NALT, we transferred either Rosa26$^{tdTomato/+}$ B1-8^{hi} or B1-8^{lo} cells, which carry BCRs specific for NP with 40-fold lower affinity, mixed with CD4$^+$ OT-II T cells, into host mice. Since the NALT has an irregular shape, we initially used activation-induced cytidine deaminase (AID) reporter host mice to visualize the location of preexisting GCs, where the transferred cells are expected to form new GC reactions (Yang Shih et al., 2002; Rommel et al., 2013). TPLSM imaging on day 5 of the response showed B cell expansion and GC seeding by B1-8^{hi} B cells, but not by B1-8^{lo} B cells in the NALT, and similar results were observed in the mediastinal LNs (MedLNs) (Fig. 1 B). We then used flow cytometry to quantify antigen-specific B cell responses and GC formation. While B1-8^{hi} B cells expanded and formed GCs, B1-8^{lo} B cells did not, as they neither expanded nor expressed GC markers in the NALT and MedLNs (Fig. 1, C and D). In a previous study, we demonstrated that antigen-specific B cells can respond in the NALT only after priming of T cells through i.p. injection of antigen or CD4$^+$ OT-II T cell transfer (Liu et al., 2024; Mao et al., 2022). To examine if T cell priming can recruit B1-8^{lo} into the GC response, we repeated this experiment using high- and low-affinity B cell clones. As expected, while B1-8^{hi} responded to the boost after T cell priming, B1-8^{lo} were unable to expand under these conditions (Fig. 1, E and F). Thus, in contrast to PPs, in which very low-affinity B clones can respond to antigen (Biram et al., 2019), in the NALT, only high-affinity variants can expand and seed GCs.

Low-affinity B cell clones are unable to seed GCs in the NALT in the absence of competition

To determine whether the inability of B1-8^{lo} B cells to form GCs depends on competition with endogenous polyclonal B cells, we transferred B1-8^{hi} or B1-8^{lo} B cells into MD4 mice, in which 99% of endogenous B cells carry an irrelevant BCR, and imaged the NALT at day 7 after NP-OVA nasal immunization (Schwickert et al., 2011). Similar to the results in WT hosts, in the absence of competition, B1-8^{lo} B cells in the NALT of MD4 mice were unable to form GCs. In contrast, B1-8^{lo} B cells were able to form GCs in the MedLNs in the absence of competition (Fig. 2, A and B). A more detailed time course analysis confirmed that B1-8^{hi} B cells but not the B1-8^{lo} B cells expanded and formed GCs at day 3 of the response. At days 5 and 7 after vaccination, B1-8^{lo} B cells were detected in the NALT of some of the mice, yet their frequency was significantly lower compared with B1-8^{hi} B cells (Fig. 2 C). B1-8^{lo} B cells were also detected on day 5 in the MedLNs, and there was no statistically significant difference on day 7 when compared with B1-8^{hi} B cells. These data confirm previous findings demonstrating the ability of low-affinity clones to form GCs in draining LNs when competition with high-affinity counterparts is lacking (Fig. 2 D) (Schwickert et al., 2011). Therefore, in contrast to PPs and MedLNs, in which very low-affinity B clones can respond to antigen (Biram et al., 2019), in the NALT, primarily high-affinity variants can expand and seed GCs, independently of interclonal competition.

To examine whether the low-affinity clones can be detected in other organs at later time points, we repeated the experiment and analyzed the presence of transferred cells in the spleen and bone marrow (BM). A small but reproducible population of B1-8^{hi} B cells was detected in the spleen of all of the MD4 mice 14 days after nasal vaccination, while in two out of six mice, B1-8^{lo} cells were detected as well; in both of these mice, the

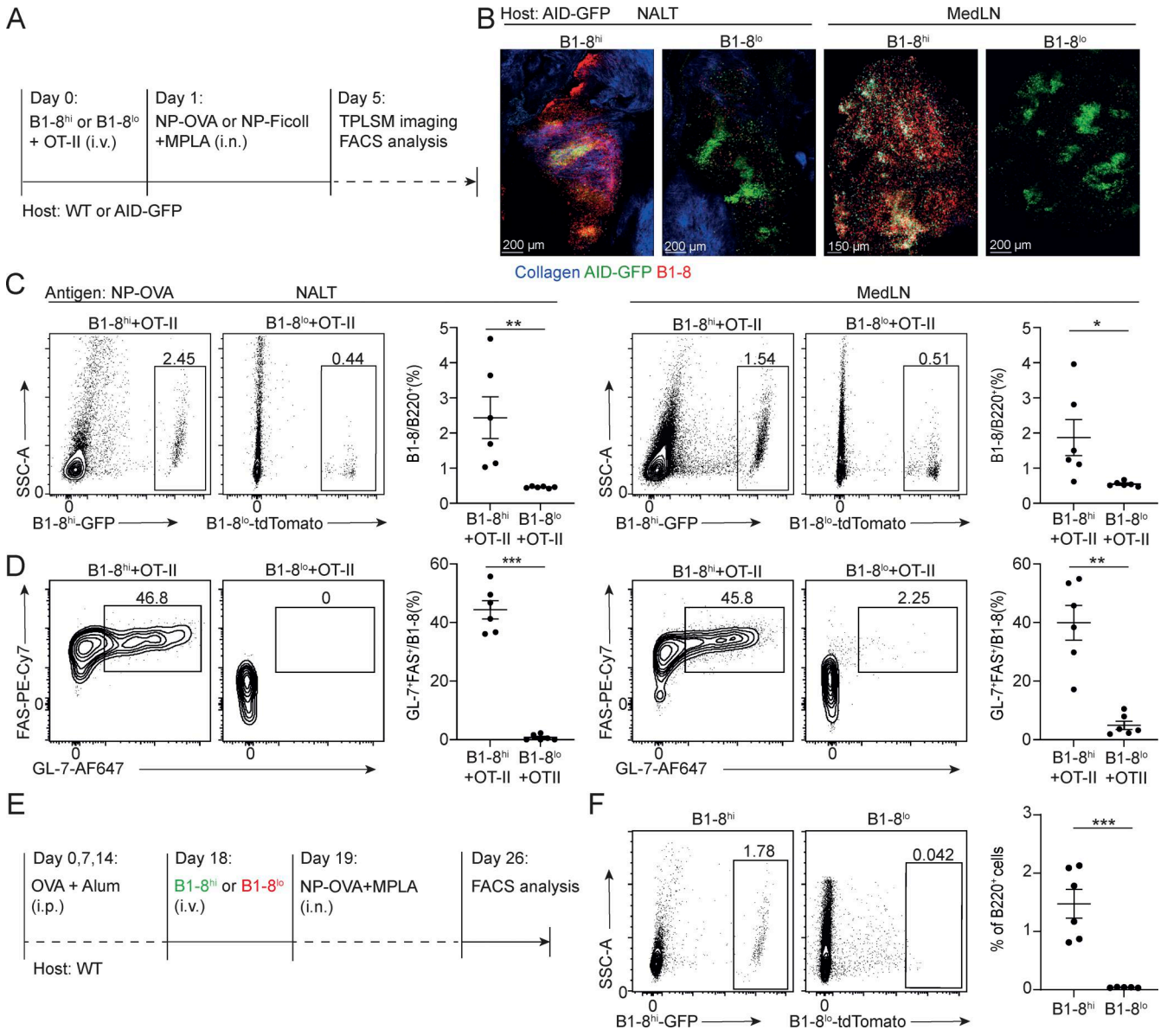

Figure 1. **B cells carrying low-affinity BCR are unable to seed GC in the NALT. (A)** Schematic representation of the experimental setup shown in B–D. **(B)** AID-GFP mice were injected with Rosa26$^{tdTomato/+}$ B1-8^{hi} or B1-8^{lo} B cells mixed with nonfluorescent CD4^{+} OT-II T cells followed by i.n. immunization with NP-OVA + MPLA. TPLSM images of NALT and MedLN 5 days following immunization are shown. *n* = 3 for each time point; two independent experiments. **(C and D)** WT mice were adaptively transferred with GFP^{+} B1-8^{hi} or Rosa26$^{tdTomato/+}$ B1-8^{lo} B cells mixed with nonfluorescent CD4^{+} OT-II T cells. LNs were analyzed by flow cytometry 5 days after i.n. NP-OVA + MPLA immunization. *n* = 6; two independent experiments. Unpaired two-tailed Student's *t* test; data represent mean ± SEM; *, P < 0.05; **, P < 0.01; ***, P < 0.001. **(E)** Experimental design for F. **(F)** Flow cytometry plots and frequency of B1-8^{hi} or B1-8^{lo} B cells 7 days after i.n. NP-OVA + MPLA boost. *n* = 6; two independent experiments. Unpaired two-tailed Student's *t* test; data represent mean ± SEM; ***, P < 0.001.

B1-8^{lo} had a GC phenotype (Fig. 2, E and F). These data suggest that initial low- and high-affinity clones have the potential to migrate to the spleen after i.n. vaccination and form GCs.

The inability of the low-affinity B cell clones to form GCs can be either a result of a lack of T cell help or ineffective BCR triggering. To examine whether low-affinity clones can respond to nonprotein antigens that are independent of T cell help, we transferred into WT mice either B1-8^{hi} or B1-8^{lo} B cells followed by nasal immunization with NP-Ficoll and MPLA. While B1-8^{hi} B cells responded to the vaccination by cell expansion, very few B1-8^{lo} B cells were detected in the NALT and MedLNs (Fig. 2 G). In addition, B1-8^{hi} B cells were able to differentiate into plasma blasts in MedLNs and in the NALT of some of the mice, while the few detected B1-8^{lo} B cells were negative for CD138 (Fig. 2 H). Thus, GC seeding and T cell–independent responses in the NALT require a minimum BCR affinity threshold.

Formation of Tfh cells in the NALT depends on BCR affinity

Proper differentiation of CD4^{+} T cells to Tfh cells requires interaction with B cells that present cognate antigen on their surface (Crotty, 2019; Baumjohann et al., 2013). We examined whether the affinity of the cognate B cell receptor regulates the

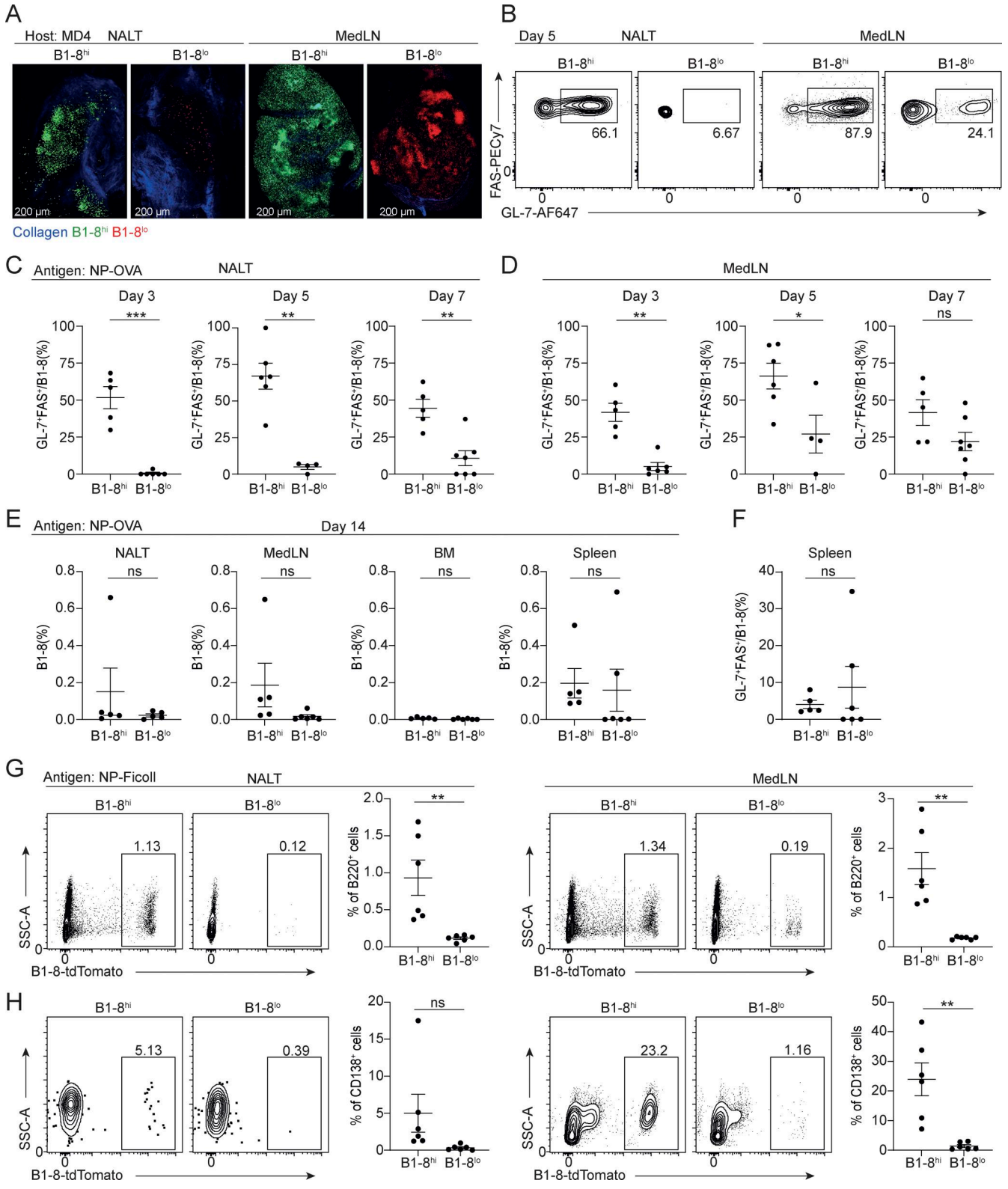

Figure 2. **Low-affinity B cell clones are unable to seed GCs in the NALT independent of competition. (A)** MD4 mice were adoptively transferred with GFP+ B1-8hi or Rosa26tdTomato/+ B1-8lo B cells. NALT and MedLN were removed and imaged by TPLSM on day 7 following i.n. NP-OVA + MPLA immunization. Scale bars, 200 µm. *n* = 4 for each time point; two independent experiments. **(B–D)** MD4 mice were injected with GFP+ B1-8hi or Rosa26tdTomato/+ B1-8lo B cells. NALT and MedLN were collected and analyzed by flow cytometry on day 3, 5, and 7 following i.n. NP-OVA + MPLA immunization. Representative plots for GC B cells on day 5 are shown (B). Flow cytometry quantification for GC B cell percentage of B1-8hi or B1-8lo B cells. Day 3, *n* = 5–6; day 5, *n* = 4–6; day 7, *n* = 5–7; six independent experiments. Unpaired two-tailed Student's *t* test; data represent mean ± SEM; *, P < 0.05; **, P < 0.01; ***, P < 0.0001; ns, not significant (C and D). **(E and F)** MD4 mice were injected with Rosa26tdTomato/+ B1-8hi or B1-8lo B cells mixed with CD45.1+ OT-II T cells. LNs, BM, and spleen were collected and

analyzed by flow cytometry on day 14 following i.n. NP-OVA + MPLA immunization. *n* = 5–6; two independent experiments. Unpaired two-tailed Student's *t* test; data represent mean ± SEM; ns, not significant. Flow cytometry quantifications for total transferred cells (E) and GC B1-8^{hi} or B1-8^{low} B cells (F) are shown. **(G and H)** WT mice were injected with Rosa26$^{tdTomato/+}$ B1-8^{hi} or B1-8^{lo} B cells. LNs were analyzed by flow cytometry 5 days after i.n. NP-Ficoll + MPLA immunization. *n* = 6; two independent experiments. Unpaired two-tailed Student's *t* test; data represent mean ± SEM; **, P < 0.01; ns, not significant.

T cell response within the NALT in WT host mice. On day 5 after immunization, the frequency of activated OT-II T cells in the NALT was 1.5-fold lower when they were transferred with B1-8^{lo} compared with B1-8^{hi} B cells; yet a significant number of OT-II T cells were detected in this structure (Fig. 3 A). In contrast, in the MedLN, more OT-II T cells were detected following B1-8^{lo} B cell transfer. Although the differences were statistically significant, they were small, and in both organs, the recovered T cells expressed activation markers (CD44^{+} and CD62L^{-}) (Fig. 3, B–D). In the NALT, the differentiation of OT-II T cells into Tfh cells was markedly less efficient in the presence of B1-8^{lo} B cells than in the presence of B1-8^{hi} B cells. These results suggest that OT-II T cells differentiate into distinct T cell subsets rather than Tfh cells when antigen-specific B cells do not respond to the cognate antigen effectively. No such difference was observed in the MedLNs (Fig. 3, E and F), which supported a polyclonal response regardless of the transferred B cells (Fig. S1, A and B). These results suggest that the two organs may differ in factors that promote Tfh cell formation, such as the presence of preexisting polyclonal response in the NALT, and the ability of the MedLN to support vaccine-induced endogenous B cell response. A time course experiment in WT hosts demonstrated that neither pre-GC nor GC Tfh cells were formed in the presence of B1-8^{lo} during the immune response (Fig. 3, G and H). B1-8^{lo} may lose to polyclonal B cells in pre-GC competition and therefore may be unable to support Tfh cell formation. To address this possibility, we repeated the experiments in MD4 mice, in which there is no competition by endogenous B cells, and found that B1-8^{lo} cells were unable to promote Tfh cell formation in this setting, as well (Fig. 3 I). Collectively, while the NALT can support T cell activation, high-affinity B cell clones are required to support Tfh cell formation.

CCR6 promotes GC formation in the NALT by high-affinity clones

In PPs, B cells upregulate CCR6, which is required for CSR to IgA, but not for GC formation, which is driven by bacterial antigens (Biram et al., 2019; Cook et al., 2000; Reboldi et al., 2016). To examine if CCR6 plays a similar role in the NALT, B1-8^{hi} B cells were transferred into WT mice, followed by nasal vaccination with NP-OVA + MPLA and flow cytometry analysis after 1–7 days. CCR6 upregulation was detected on day 3 of the response, and expression of this receptor was detected on most responding B cells 7 days after vaccination (Fig. 4 A). FAS^{+} CD38^{+} B1-8^{hi} B cells expressed CCR6, which was downregulated in GC B cells (FAS^{+}, CD38^{-}) (Fig. 4 B). B1-8^{lo} B cells were unable to expand in response to nasal immunization and did not express CCR6 early during the response. Yet, on day 7, CCR6 was detected on a few B1-8^{lo} B cells, suggesting that a delayed response might have occurred (Fig. 4 B). Thus, B cells with high-affinity BCRs effectively upregulate CCR6 and participate in the immune response in the NALT.

To examine the role of CCR6, we crossed B1-8^{hi}-transgenic mice with CCR6-deficient mice. Using adoptive cell transfer and TPLSM, we detected CCR6-deficient B1-8^{hi} cells in the NALT in response to nasal vaccination on days 3–7 of the response, though in a smaller number compared with CCR6$^{+/+}$ B1-8^{hi} B cells (Fig. 4 C). To accurately quantify GC responses, we repeated the experiment and examined the transferred cells by using flow cytometry. This analysis revealed that CCR6-deficient B1-8^{hi} cells expand and differentiate to GC B cells in response to nasal vaccination, less effectively than CCR6$^{+/+}$ B1-8^{hi} B cells (Fig. 4, D and E; and Fig. S1, C–F). In addition, OT-II T cells were unable to expand and form Tfh cells in the presence of CCR6-deficient B1-8^{hi} B cells (Fig. 4, F and G). Collectively, these experiments show that B cell CCR6 is required for effective GC seeding and Tfh formation in the NALT in response to nasal vaccination.

Efficient CSR to IgA in the NALT requires B cell SED localization mediated by CCR6

In PPs, CSR to IgA depends on CCR6 expression, which guides B cells to the SED (Reboldi et al., 2016; Biram et al., 2019; Cook et al., 2000). To determine if CCR6 plays a similar role in the NALT, we first examined the location of WT and CCR6-deficient B1-8^{hi} B cells in this organ. We previously demonstrated that antigen-specific B cells initially proliferate and form large cell clusters in the SED of the NALT and PPs (Liu et al., 2024; Biram et al., 2019). Using CX$_3$CR1-GFP reporter mice and based on morphological analysis, we demonstrated that macrophages reside in the SED in both the NALT and are distributed among the expanded CCR6$^{+/+}$ antigen-specific B cells (Fig. 5 A) (Biram et al., 2019). Together with our previous findings (Liu et al., 2024), these data confirm that the transferred antigen-specific B cells translocate to the SED in the NALT.

To determine if CCR6 directs B cells to the SED in the NALT, we first examined the location of WT and CCR6-deficient B1-8^{hi} B cells in the NALT using AID reporter mice, in which B cells expressing, or that previously expressed AID are tdTomato^{+}. On day 5 of the response, large clusters of transferred CCR6$^{+/+}$ B1-8^{hi} B cells were detected next to the nasal lumen, distant from the endogenous tdTomato^{+} GC B cells. These clusters represent the SED microanatomical site within the NALT (Liu et al., 2024). In contrast, CCR6-deficient B1-8^{hi} B cells were unable to form these clusters and were scattered throughout the organ (Fig. 5 B). To link CCR6 and cell location to IgA CSR, we stained transferred B1-8^{hi} B cells for surface IgA at days 5 and 7 after i.n. vaccination. CCR6 deficiency had an insignificant effect on B cell expansion on day 5 of the response, yet the frequency of IgA^{+} GC B cells was significantly reduced (Fig. 5, C and D). Analysis of all transferred B1-8^{hi} B cells on day 7 after vaccination, including all B cell subtypes, and GC B cells in particular, demonstrated a defect in CSR to IgA in CCR6-deficient B cells (Fig. 5, E and F). Thus, CCR6

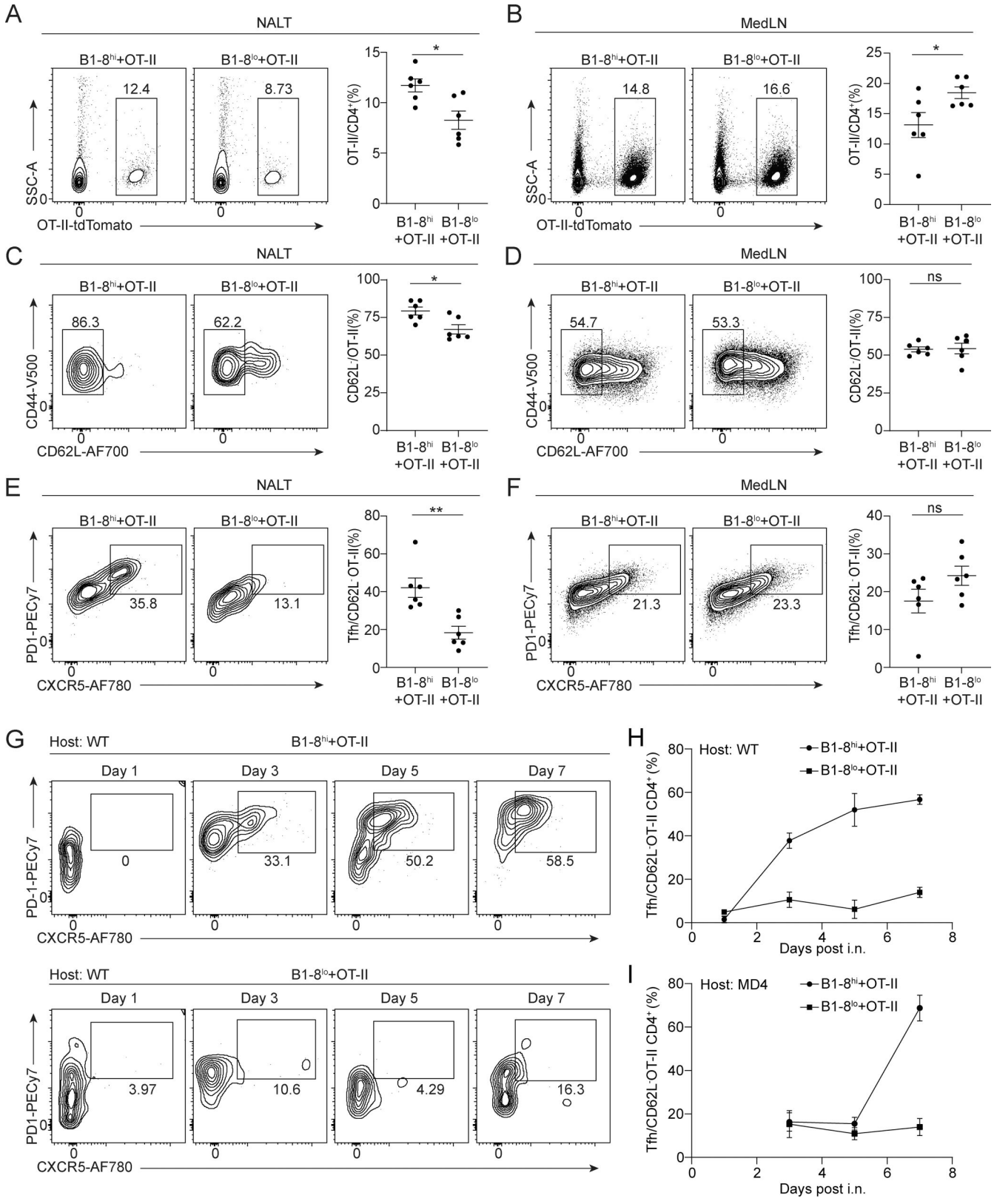

Figure 3. **Formation of Tfh cells in the NALT depends on BCR affinity. (A–F)** WT mice were injected with GFP$^+$ B1-8^{hi} or Rosa26$^{tdTomato/+}$ B1-8^{lo} B cells mixed with CD45.1$^+$ OT-II T cells. Flow cytometry analysis of OT-II T cells was performed at day 5 following i.n. NP-OVA + MPLA immunization. *n* = 6; two independent experiments. Unpaired two-tailed Student's *t* test; data represent mean ± SEM. *, P < 0.05; **, P < 0.01; ns, not significant. Flow cytometry plots and quantification of total OT-II T cells (A and B), activated CD44$^+$ CD62L$^-$ OT-II T cells (C and D), CXCR5$^+$ PD-1$^+$ Tfh cells out of activated OT-II T cells (E and F) are shown. **(G and H)** Time course analysis of Tfh OT-II T cells formation in WT mice as in A. Day 1 *n* = 3; day 3, *n* = 3; day 5 *n* = 3; day 7 *n* = 2–3; one experiment. Unpaired two-tailed Student's *t* test; data represent mean ± SEM. **(I)** Same experiment as in G using MD4 hosts. Day 3, *n* = 5–6; day 5, *n* = 8–9; day 7, *n* = 2–4; three independent experiments. Unpaired two-tailed Student's *t* test; data represent mean ± SEM.

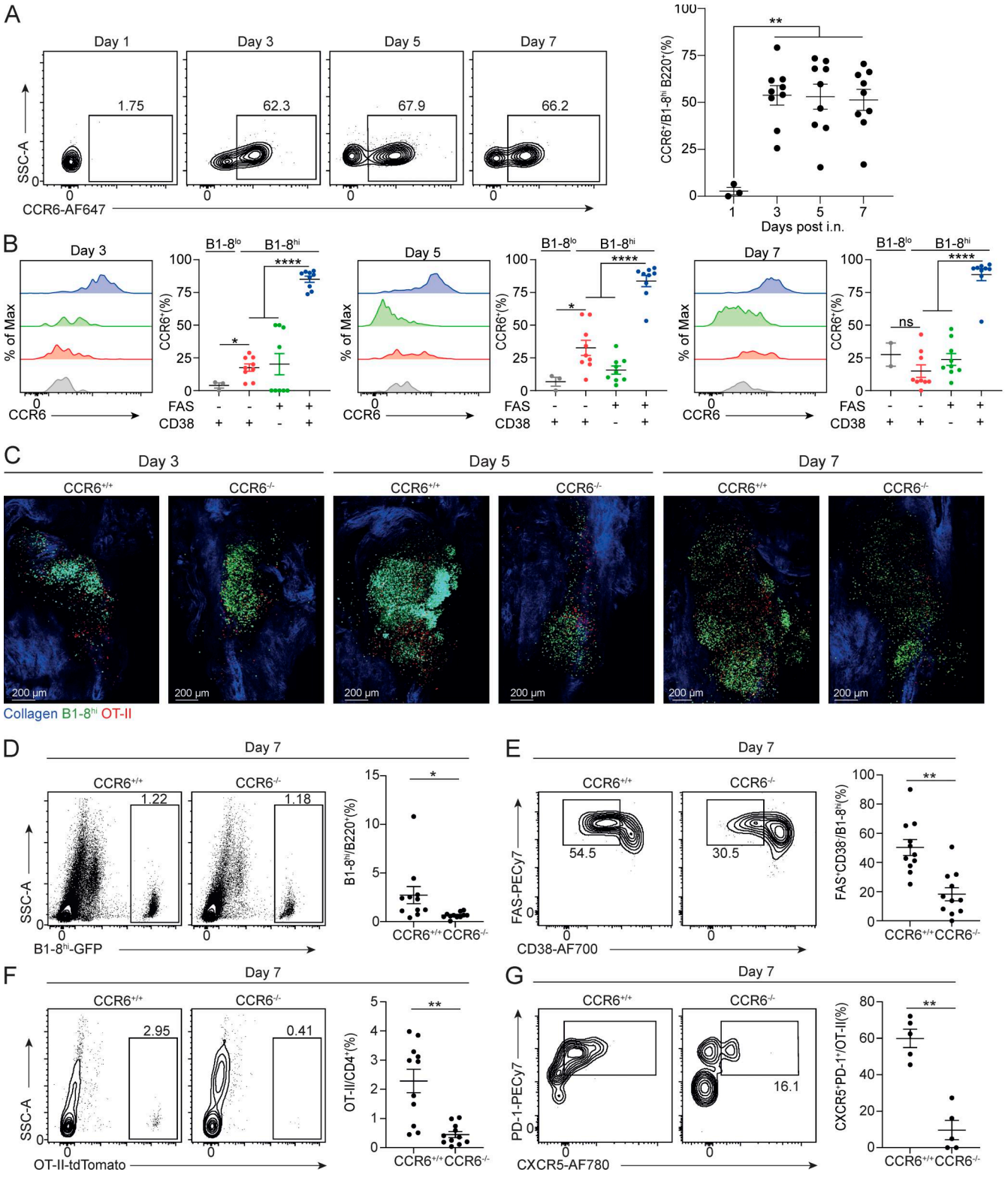

Figure 4. **GC formation by high-affinity B cell clones depends on CCR6 expression. (A)** WT mice were adoptively transferred with GFP$^+$ B1-8^{hi} B cells and CD45.1$^+$ OT-II T cells. CCR6 expression on B1-8^{hi} B cells was assessed by flow cytometry at the indicated time points after i.n. NP-OVA + MPLA immunization. Day 1, n = 3; day 3, n = 9; day 5, n = 9; day 7, n = 9; three independent experiments. Data represent mean ± SEM. **(B)** WT mice were adoptively transferred with GFP$^+$ B1-8^{hi} or Rosa26$^{tdTomato/+}$ B1-8^{lo} B cells, together with CD45.1$^+$ OT-II T cells. The frequency of CCR6 expressing B1-8^{hi} and B1-8^{lo} B cells was analyzed by flow cytometry at the indicated time points. Day 3, n = 3–9; day 5, n = 3–9; day 7, n = 2–9; three independent experiments. Data represent mean ± SEM. **(C)** WT mice were adoptively transferred with GFP$^+$ CCR6$^{+/+}$ or CCR6$^{-/-}$ B1-8^{hi} B cells, and Rosa26$^{tdTomato/+}$ OT-II T cells. NALTs were imaged on days 3, 5, and 7 after i.n. NP-OVA + MPLA immunization, using TPLSM. Scale bars, 200 µm. For each time point, n = 2–4 mice; two independent experiments. **(D–G)** WT mice were adoptively transferred with GFP$^+$ CCR6$^{+/+}$ or CCR6$^{-/-}$ B1-8^{hi} B cells and Rosa26$^{tdTomato/+}$ OT-II T cells. Transferred cells (D), GC B cells (E), OT-II T cells (F), and OT-II Tfh T cells (G) subsets were quantified by flow cytometry on day 7 following i.n. NP-OVA + MPLA immunization. n = 5–11; three independent experiments. Unpaired two-tailed Student's t test; data represent mean ± SEM; *, P < 0.05; **, P < 0.01; ****, P < 0.0001.

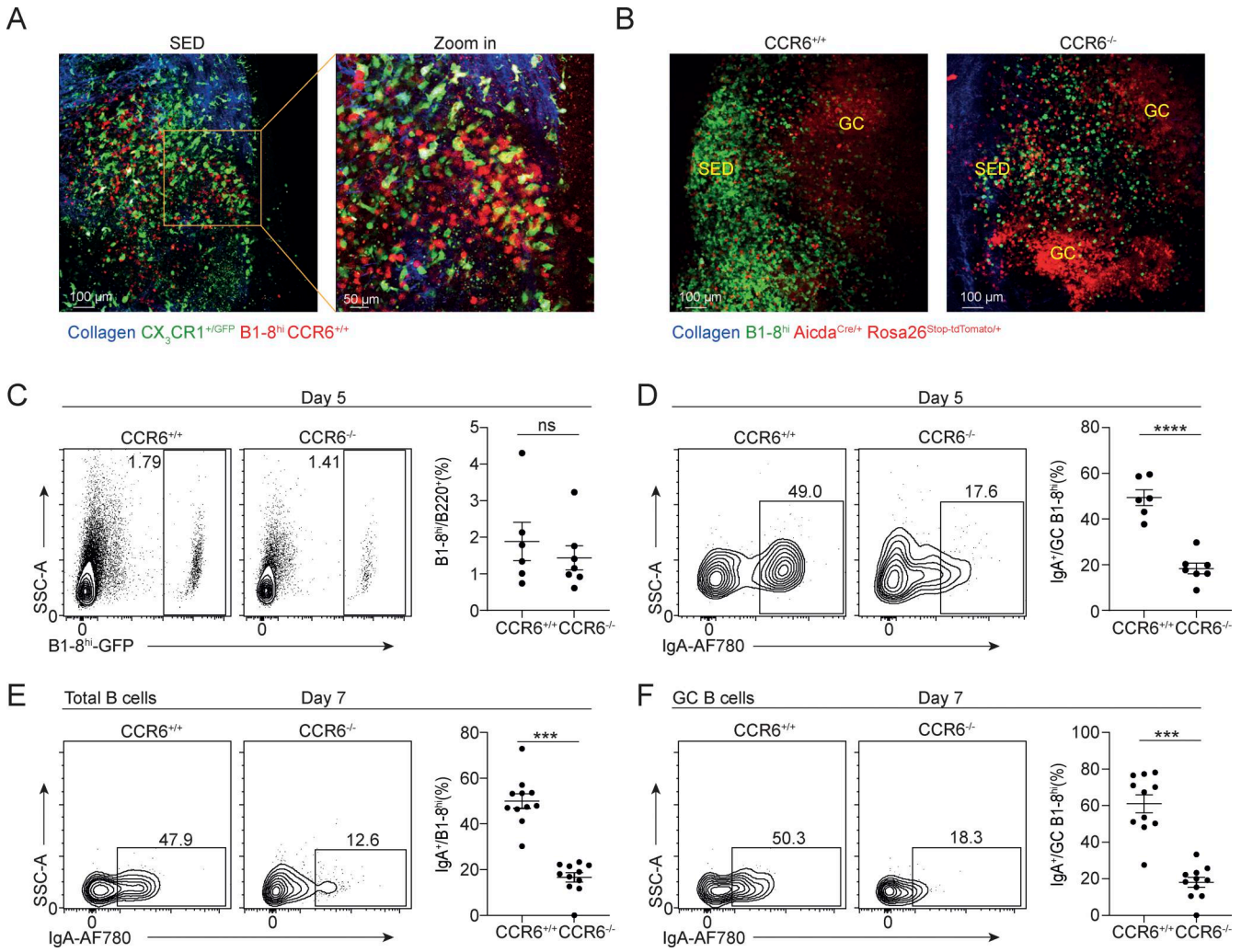

Figure 5. **IgA class switching in the NALT depends on CCR6-mediated B cell positioning in the SED. (A)** CX_3CR1-GFP mice were adoptively transferred with Rosa26$^{tdTomato/+}$ B1-8^{hi} B cells and CD45.1$^+$ OT-II T cells. NALTs were imaged on day 5 after i.n. NP-OVA + MPLA immunization using TPLSM. Scale bars, 50–100 µm. *n* = 2; one experiment. **(B)** Aicda$^{Cre/+}$ Rosa26$^{Stop\text{-}tdTomato/+}$ mice were adoptively transferred with GFP$^+$ CCR6$^{+/+}$ or CCR6$^{-/-}$ B1-8^{hi} B cells and CD45.1$^+$ OT-II T cells. NALTs were imaged on day 5 after i.n. NP-OVA + MPLA immunization using TPLSM. Scale bars, 100 µm. *n* = 3; one experiment. **(C–F)** WT mice were adoptively transferred with GFP$^+$ CCR6$^{+/+}$ or CCR6$^{-/-}$ B1-8^{hi} B cells and OT-II T cells followed by NP-OVA + MPLA i.n. immunization. Transferred B1-8^{hi} B cells (C) and IgA$^+$ GC subsets (D) were quantified by flow cytometry on day 5; the frequency of IgA$^+$ B cells was quantified out of the total transferred cells (E) or GC B cells (F) on day 7. Day 5, *n* = 6–7; day 7, *n* = 11; four independent experiments. Unpaired two-tailed Student's *t* test; Data represent mean ± SEM; ***, P < 0.001; ****, P < 0.0001; ns, not significant.

is necessary for B cell positioning in the SED and effective CSR to IgA in the NALT.

CCR6 is required for the formation of IgA GC B cells in the NALT in response to commensal bacteria

Our findings using transgenic immune cells indicate that CCR6 plays a significant role in B cell immune responses in the NALT. Affinity-based clonal selection was previously demonstrated in response to orally delivered antigens and in response to commensal bacteria in a polyclonal immune response in PPs (Nowosad et al., 2020; Chen et al., 2020; Biram et al., 2019). To investigate the role of CCR6 in a polyclonal immune response to commensal bacteria within the NALT, we examined its function in B cells responding to these bacteria. We previously demonstrated that in the NALT of germ-free (GF) mice, GCs were smaller compared with those in specific pathogen–free (SPF) mice (Liu et al., 2024). In PPs, the most abundant BCR isotypes are IgA and IgG1 (Riedel et al., 2020; Lycke and Bemark, 2012); however, in the NALT, IgG2b was more abundant than IgA, and no IgG1$^+$ GC B cells were detected (Fig. 6 A). In addition, in GF mice, most of the B cells in the PPs expressed IgG1 (Nowosad et al., 2020; Chen et al., 2020; Biram et al., 2019), whereas the NALT B cells lacked IgG1 and mainly expressed IgG2b (Fig. 6 A). While IgA is expected to be specific to commensals, less data are available about the ability of IgG2b to bind bacteria. It was shown that, following antibiotic treatment, IgG2b$^+$ B cells are reduced in PPs, and commensal-reactive bacteria in the sera are diminished as well (Okada et al., 2025) and IgG2b$^+$ B cell found in cecal patches show bacteria-binding activity (Tsuda et al., 2022). It is most likely that the IgG2b in the NALT functions in a similar manner.

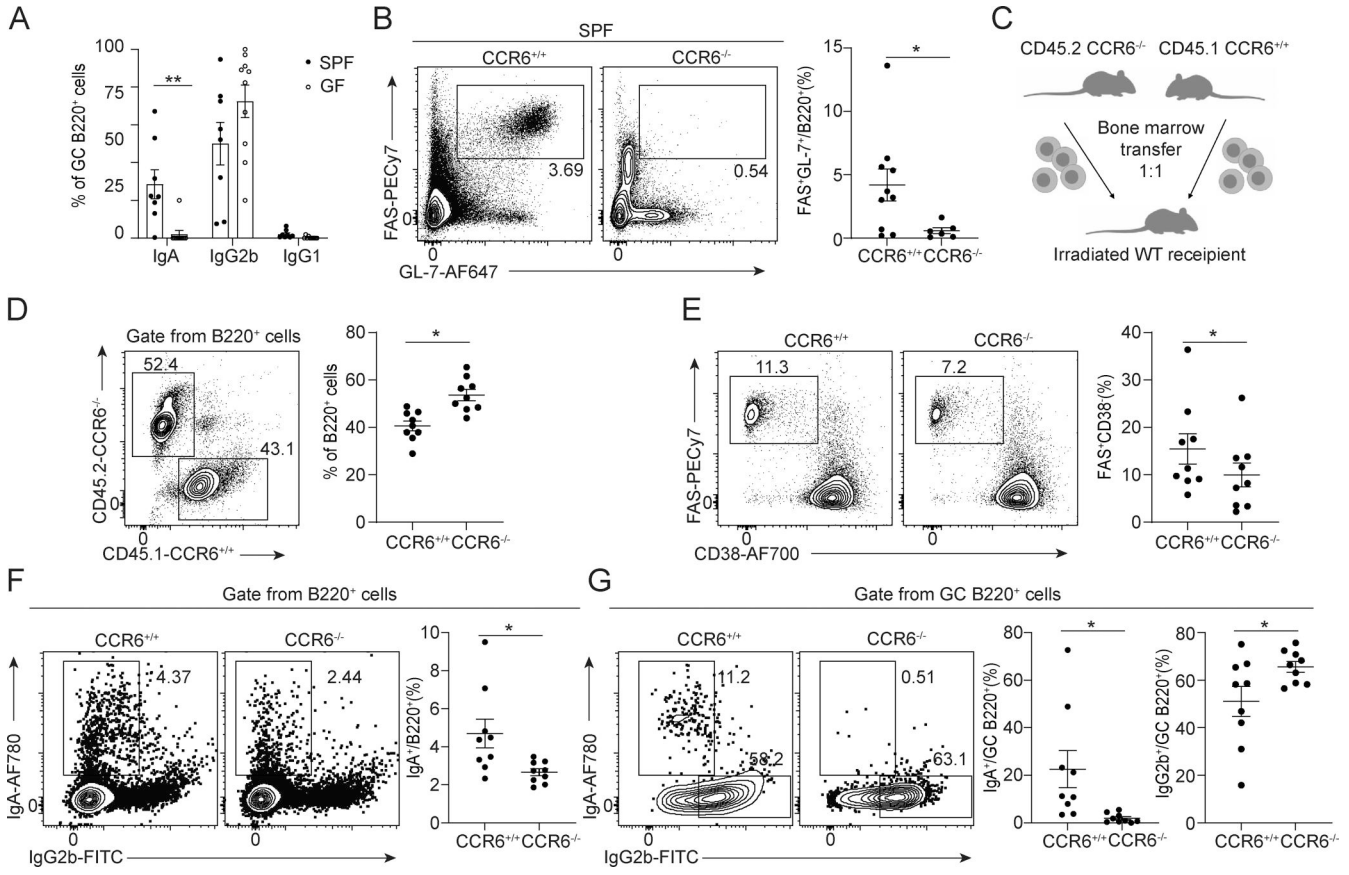

Figure 6. **CCR6 is required for bacteria-driven IgA GC B cell formation in the NALT. (A)** Quantification by flow cytometry of B cell isotypes in NALTs from SPF or GF mice under homeostasis. IgA⁺, IgG2b⁺, and IgG1⁺ populations were gated from Fas⁺CD38⁻B220⁺ GC B cells. *n* = 8–10; two independent experiments. Unpaired two-tailed Student's *t* test; data represent mean ± SEM; **, P < 0.01. **(B)** Flow cytometry analysis of GC B cells in NALT from CCR6$^{+/+}$ or CCR6$^{-/-}$ SPF mice. *n* = 6–10; three independent experiments. Unpaired two-tailed Student's *t* test; data represent mean ± SEM; *, P < 0.05. **(C)** Experimental design of mixed BM chimeras generated with CCR6$^{+/+}$ and CCR6$^{-/-}$ donors. **(D–G)** Flow cytometry analysis of B cell subsets in NALTs from BM chimeras. CCR6$^{+/+}$ and CCR6$^{-/-}$ B cells were gated from B220⁺ B cells (D); GC (Fas⁺CD38⁻) B cell populations were gated from CCR6$^{+/+}$ or CCR6$^{-/-}$ B220⁺ cells in D (E); IgA⁺ and IgG2b⁺ populations were gated from CCR6$^{+/+}$ or CCR6$^{-/-}$ B220⁺ cells (F), or from CCR6$^{+/+}$ or CCR6$^{-/-}$ GC B cells (G). *n* = 9; two independent experiments. Paired two-tailed Student's *t* test; data represent mean ± SEM; *, P < 0.05.

To examine the contribution of CCR6 to CSR in a polyclonal immune response against commensal bacteria, we compared GCs in WT and CCR6-deficient SPF mice and found that the latter lacks GC B cells in their NALTs (Fig. 6 B), similar to the PPs in mice that globally lacks CCR6 (Cook et al., 2000; Reboldi et al., 2014; Biram et al., 2019). Thus, in contrast to an approach based on transgenic B cells, we were unable to examine IgA expression in bacteria-driven GC B cells within these CCR6-deficient mice. CCR6 is expressed on several cell types, including B cells, which may affect the outcome of this experiment. To overcome this problem, we reconstituted irradiated WT mice with mixed BM cells derived from CCR6-WT and CCR6-deficient mice (~50% of each BM) (Fig. 6 C). Indeed, under these conditions, GCs were formed by both WT and CCR6-deficient B1-8^{hi} B cells, demonstrating that the defect in CCR6-deficient cells was B cell extrinsic (Fig. 6, D and E). However, the frequency of CCR6-deficient B cells in the GC was slightly lower compared with WT (Fig. 6 E). The frequency of total IgA⁺ B cells in the NALT was lower in the CCR6-deficient B cell population, yet a clear cell population was detected (Fig. 6 F). Nonetheless, nearly no IgA⁺ GC B cells were detected among the CCR6-deficient cell population (Fig. 6 G). In contrast, there was no reduction in the frequency of IgG2b⁺ GC B cells, and, in fact, their percentage was increased due to a decrease in IgA⁺ GC B cells (Fig. 6 G). Thus, CCR6 is required for the formation of IgA but not IgG2b⁺ GC B cells in response to commensal bacteria in the NALT.

Discussion

Antibody-secreting cells are crucial for protecting mucosal surfaces from harmful pathogens and for maintaining balance with commensal bacteria (Oh et al., 2021). Although the main principles of B cell immune responses are similar between mucosal tissues and typical draining LNs, some important differences exist (Biram et al., 2019; Biram et al., 2020; Reboldi and Cyster, 2016). Here, we show that B cells with low-affinity BCRs cannot respond to antigen nor upregulate CCR6 in the NALT and form IgA⁺ GC B cells. Our findings suggest that effective antigen receptor triggering in the NALT is linked to proper B cell positioning in the NALT SED, where CSR to IgA occurs.

Although the B1-8^{lo} B cells had the potential to respond to the NP antigen, as shown in previous studies in draining LNs and PPs (Schwickert et al., 2009; Biram et al., 2019) and demonstrated here in MedLN of MD4 mice, they did not respond to the nasal vaccination in the NALT. These findings indicate that a minimal affinity is required for response to an antigen in this organ and suggest that high levels of antigen or continuous antigen availability are needed when using nasal vaccine for the activation of low-affinity clones (Cirelli et al., 2020). A limitation of using B1-8^{lo} B cells is that they express extremely low-affinity BCRs, and it is most likely that cells bearing intermediate-affinity receptors are able to respond to the antigen in the upper airways.

Our study revealed several factors shared between the NALT and the PPs. Both organs support IgA CSR in a manner dependent on CCR6, a GPCR that attracts cells to the SED niche (Cook et al., 2000). It is most likely that the SED of the NALT contains all cell types and molecules supporting CSR to IgA, including TGFβ, cells expressing αVβ8, and Rorγt^{+} innate lymphoid cells (Reboldi and Cyster, 2016). In addition, the finding reveals some differences between the two organs: in PPs, low-affinity B cells can expand in the SED but cannot seed GCs, while in NALT, they do not expand at all, even in the absence of competing B cells (Biram et al., 2019). Using adoptive cell transfer and vaccination, we show that, similar to PPs, most GC B cells express IgA in response to vaccination with cognate antigen in the NALT. However, in contrast to PPs, in a polyclonal response, most NALT GC B cells, driven by commensal bacteria, express IgG2b rather than IgG1. These observations suggest that a different "natural" adjuvant drives the commensal-driven response in NALT compared with the PPs.

We and others showed that while GC formation in response to commensal bacteria is not CCR6-dependent, vaccine-induced GCs require this GPCR in both the NALT and PPs (Reboldi et al., 2016; Biram et al., 2019). The NALT is a very small structure compared with PPs, and exposure to antigen delivered by vaccination is expected to be very inefficient compared with chronic stimulation by commensal bacteria or replicating virus (Davis, 2001). Therefore, CCR6 expression and localization within the SED may enable B cell exposure to antigen for longer periods within the NALT tissue. Ectopic GCs were detected in the nasal cavity and in the lungs; however, since they are not part of a defined lymphoid organ, they lack SED in their proximity (Gailleton et al., 2025; Denton et al., 2019). Nonetheless, these GCs may recruit IgA^{+} memory B cells that were formed in SED-containing lymphoid organs or support rare events of sequential CSR (Siniscalco et al., 2025). CSR to IgA in the PPs can take place without T cell help, but no GCs are formed or when T cell help is sub-optimal (Biram et al., 2020; Bergqvist et al., 2006; Bergqvist et al., 2010). IgA-expressing non-GC B cells were found in the NALT despite lacking CCR6, suggesting that IgA CSR may occur through other pathways, potentially involving sequential CSR (Siniscalco et al., 2025). Furthermore, IgA^{+} B cells can be formed by a specific cell subset known as type 1 Tfh cells, which can be primed by B cells (Haniuda et al., 2025). It is most likely that the formation of these Tfh cells depends on BCR affinity, high level of antigen presentation, and CCR6, as well.

Overall, our findings might have implications for the development of mucosal immunizations and suggest that a large antigen dose or a nasal vaccine with sustained release of antigen in the upper airways might be more effective in promoting the activation of B cells that carry lower affinity BCRs in the SED (Cirelli et al., 2020). Thus, developing nasal immunization that targets high-affinity B cell clones or with a prolonged antigen exposure period may facilitate the recruitment of antigen-specific B cells to the SED and provide more effective vaccine-induced protection (Topol and Iwasaki, 2022).

Materials and methods

Mice

Transgenic Igλ B1-8^{hi} and Igλ B1-8^{lo} knock-in mice were provided by M.C. Nussenzweig (The Rockefeller University, New York, NY, USA). AID-GFP mice were generated by R. Casellas (National Institute of Arthritis and Musculoskeletal and Skin Diseases, National Institutes of Health, Bethesda, MD, USA) and obtained from M.C. Nussenzweig. CD45.1 congenic mice were provided by R. Alon (Weizmann Institute of Science, Rehovot, Israel). GF mice were provided by E. Elinav (Weizmann Institute of Science, Rehovot, Israel). CX_3CR1-GFP mice were provided by S. Jung (Weizmann Institute of Science, Rehovot, Israel). CCR6$^{-/-}$, GFP^{+}, Rosa26$^{tdTomato/+}$, OT-II, and MD4 transgenic mice were purchased from The Jackson Laboratory. GFP^{+} and Rosa26^{tdTomato}-expressing mice (with a germline deletion of the stop codon) were crossed to Igλ B1-8^{hi} and B1-8^{lo} or OT-II mice. C57BL/6 wild-type mice were purchased from Harlan Laboratories. For the generation of CD45.2 CCR6$^{-/-}$ and CD45.1 CCR6$^{+/+}$ mixed chimeric mice, WT hosts were irradiated with 950 rad and then reconstituted with mixed BM cells at a 1/1 ratio. Mice were used 8 wk after BM reconstitution. All mice were maintained under SPF conditions in the Weizmann Institute animal facility at 18–23°C, 40–60% humidity, and a 12-h light/dark cycle. Host mice were all male (8–12 wk old), while donor mice were male (OT-II, B1-8^{hi}, and B1-8^{lo}) or female (B1-8^{hi} and B1-8^{lo}). All procedures were performed in accordance with protocols approved by the Weizmann Institutional Animal Care and Use Committee.

Adoptive cell transfer

Single-cell suspensions were prepared by gently pressing spleens through a 70-µm cell strainer (BD Biosciences) into PBS containing 2% FBS (Gibco) and 1 mM EDTA. CD4^{+} T cells were isolated using the CD4^{+} T Cell Isolation Kit (130-104-454; Miltenyi). B cells were purified by negative selection with anti-CD43 microbeads (130-049-801; Miltenyi). For Igλ^{+} B cell enrichment, cells were incubated with anti-Igκ-PE antibody (BioLegend) for 30 min at 4°C, washed, and Igκ^{+} cells were depleted using anti-PE microbeads (130-048-801; Miltenyi). Enrichment of Igλ^{+} cells was confirmed by flow cytometry. Purified cells (1×10^6 total; 0.5×10^6 of each population, or 0.5×10^6 of a single population) were resuspended in 100 µl PBS and transferred intraorbitally into anesthetized recipient mice.

i.n. immunizations

NP-OVA (Cat# N-5051-100; NP_{15}-OVA, Biosearch Technologies) and NP-Ficoll (Cat# F-1420-10; NP_{46}-AECM-FICOLL, Biosearch

Technologies) were used as antigens, and MPLA (Cat# 699800P; Avanti Polar Lipids) served as a mucosal adjuvant. Mice were anesthetized, placed in a supine position, and immunized i.n. with 30 µl PBS containing 10 µg NP-OVA or NP-Ficoll and 20 µg MPLA (15 µl per nostril). Immunizations were performed 8–24 h after adoptive cell transfer.

Lymphoid organ dissection

NALTs were dissected as described previously (Liu et al., 2024). Mice were euthanized by cervical dislocation, and the lower jaw and tongue were removed. Heads were rinsed in ice-cold PBS and pinned to a wax dissection surface to expose the upper palate. Palates were excised with a no. 15 scalpel blade and gently separated from surrounding tissues by gripping behind the incisors with fine forceps and freeing tissue between the palate, jawbones, and nasal septum. For MedLN isolation, the diaphragm was incised, and the lower ribs were opened to the level of the thymus. Ribs were retracted and pinned to expose the thoracic cavity, the lung was gently displaced to the right, and the MedLN, located beneath the heart and adjacent to the ventral trachea, was excised with fine forceps.

Flow cytometry

LNs were dissected as described above and passed through a 70-µm cell strainer (BD Biosciences) into ice-cold FACS buffer (2% FBS and 1 mM EDTA in PBS). Single-cell suspensions were incubated with 2 µg/ml anti-CD16/32 (clone 93) for 5 min to block Fc receptors, washed, and stained for 30 min at 4°C with the following fluorochrome-conjugated antibodies (all from BioLegend). B cell panel: B220 PB, Fas PE/Cy7, CD38 AF 700, GL-7 PerCP5.5, CD138 BV605, IgA biotin + streptavidin–AF780, and CCR6 APC; T cell panel: CD45.1 APC, CD4 PB, CD44 V500, CD62L AF 700, CXCR5 biotin + streptavidin– AF780, and PD-1 PE/Cy7. GC B cells were defined as live/single $B220^{+}CD38^{lo}Fas^{hi}$, plasma cells as $B220^{med}CD138^{+}$, and Tfh cells as $CXCR5^{+}PD\text{-}1^{+}CD62L^{-}CD4^{+}$. $tdTomato^{+}$ cells were detected in the PE channel. Samples were acquired on a CytoFLEX flow cytometer (Beckman Coulter) and analyzed by FlowJo (version 10.7.2) using standard gating strategies.

TPLSM imaging

Imaging was performed using a TPLSM Zeiss LSM 880 upright microscope equipped with a Coherent Chameleon Vision II femtosecond-pulsed laser tuned to 940 nm. Emission was split with a 565 LPXR dichroic beamsplitter to a PMT detector (579–631-nm bandpass filter for tdTomato) and with an additional 505 LPXR mirror to two GaAsP detectors (500–550 nm for GFP/FITC, 460–480 nm for CFP). Dissected NALT and MedLN were placed in PBS on a coverslip and imaged with a 20×/1.05 NA Plan Apo objective (Zeiss). Images were acquired as 80–150-µm z-stacks with 10–15-µm steps, using a zoom of 1.5 and 512 × 512 resolution in the xy plane.

Statistical analysis

All the graphs were prepared, and statistical analyses were performed using GraphPad Prism (Version 10.0). The data in the figures are reported as mean ± SEM, and the P value, number of experiments, and mice used are provided in the figure legends. The statistical analysis was performed using Student's *t* test.

Online supplemental material

Fig. S1 includes data on polyclonal B cell responses (A and B) and flow cytometry analyses comparing immunized and unimmunized mice that received CCR6-deficient $B1\text{-}8^{hi}$ B cells (C–F). Data in Fig. S1, A and B are related to Fig. 1, C and D; and Fig. 3, A–F.

Data availability

All data supporting the findings of this study are available within the main text and supplemental material. Additional raw flow cytometer and imaging data are also available upon reasonable request from the corresponding authors.

Acknowledgments

Z. Shulman is supported by the European Research Council grant no. 101001613, Israel Science Foundation grant no. 1090/18, and the Morris Kahn Institute for Human Immunology. Z. Shulman is a member of the European Molecular Biology Organization Young Investigator Program.

Author contributions: Jingjing Liu: conceptualization, data curation, formal analysis, investigation, methodology, supervision, validation, visualization, and writing—original draft, review, and editing. Liat Stoler-Barak: supervision and writing—review and editing. Ziv Shulman: conceptualization, funding acquisition, project administration, resources, supervision, validation, and writing—original draft, review, and editing.

Disclosures: The authors declare no competing interests exist.

Submitted: 16 September 2025
Revised: 24 November 2025
Accepted: 20 January 2026

References

Agace, W.W., and K.D. McCoy. 2017. Regionalized development and maintenance of the intestinal adaptive immune landscape. *Immunity*. 46: 532–548. https://doi.org/10.1016/j.immuni.2017.04.004

Baumjohann, D., S. Preite, A. Reboldi, F. Ronchi, K.M. Ansel, A. Lanzavecchia, and F. Sallusto. 2013. Persistent antigen and germinal center B cells sustain T follicular helper cell responses and phenotype. *Immunity*. 38: 596–605. https://doi.org/10.1016/j.immuni.2012.11.020

Bemark, M., M.J. Pitcher, C. Dionisi, and J. Spencer. 2024. Gut-associated lymphoid tissue: A microbiota-driven hub of B cell immunity. *Trends Immunol.* 45:211–223. https://doi.org/10.1016/j.it.2024.01.006

Bergqvist, P., E. Gärdby, A. Stensson, M. Bemark, and N.Y. Lycke. 2006. Gut IgA class switch recombination in the absence of CD40 does not occur in the lamina propria and is independent of germinal centers. *J. Immunol.* 177:7772–7783. https://doi.org/10.4049/jimmunol.177.11.7772

Bergqvist, P., A. Stensson, L. Hazanov, A. Holmberg, J. Mattsson, R. Mehr, M. Bemark, and N.Y. Lycke. 2012. Re-utilization of germinal centers in multiple Peyer's patches results in highly synchronized, oligoclonal, and affinity-matured gut IgA responses. *Mucosal Immunol.* 6:122–135. https://doi.org/10.1038/mi.2012.56

Bergqvist, P., A. Stensson, N.Y. Lycke, and M. Bemark. 2010. T cell-independent IgA class switch recombination is restricted to the GALT and occurs prior to manifest germinal center formation. *J. Immunol.* 184: 3545–3553. https://doi.org/10.4049/jimmunol.0901895

Biram, A., J. Liu, H. Hezroni, N. Davidzohn, D. Schmiedel, E. Khatib-Massalha, M. Haddad, A. Grenov, S. Lebon, T.M. Salame, et al. 2022. Bacterial infection disrupts established germinal center reactions through monocyte recruitment and impaired metabolic adaptation. *Immunity*. 55: 442–458.e8. https://doi.org/10.1016/j.immuni.2022.01.013

Biram, A., A. Strömberg, E. Winter, L. Stoler-Barak, R. Salomon, Y. Addadi, R. Dahan, G. Yaari, M. Bemark, and Z. Shulman. 2019. BCR affinity differentially regulates colonization of the subepithelial dome and infiltration into germinal centers within Peyer's patches. *Nat. Immunol.* 20: 482–492. https://doi.org/10.1038/s41590-019-0325-1

Biram, A., E. Winter, A.E. Denton, I. Zaretsky, B. Dassa, M. Bemark, M.A. Linterman, G. Yaari, and Z. Shulman. 2020. B cell diversification is uncoupled from SAP-mediated selection forces in chronic germinal centers within Peyer's patches. *Cell Rep.* 30:1910–1922.e5. https://doi.org/10.1016/j.celrep.2020.01.032

Bonnardel, J., C. Da Silva, S. Henri, S. Tamoutounour, L. Chasson, F. Montañana-Sanchis, J.-P. Gorvel, and H. Lelouard. 2015. Innate and adaptive immune functions of Peyer's patch monocyte-derived cells. *Cell Rep.* 11: 770–784. https://doi.org/10.1016/j.celrep.2015.03.067

Chen, H., Y. Zhang, A.Y. Ye, Z. Du, M. Xu, C.-S. Lee, J.K. Hwang, N. Kyritsis, Z. Ba, D. Neuberg, et al. 2020. BCR selection and affinity maturation in Peyer's patch germinal centres. *Nature*. 582:421–425. https://doi.org/10.1038/s41586-020-2262-4

Cirelli, K.M., D.G. Carnathan, B. Nogal, J.T. Martin, O.L. Rodriguez, A.A. Upadhyay, C.A. Enemuo, E.H. Gebru, Y. Choe, F. Viviano, et al. 2020. Slow delivery immunization enhances HIV neutralizing antibody and germinal center responses via modulation of immunodominance. *Cell*. 180:206. https://doi.org/10.1016/j.cell.2019.12.027

Coates, M.L., N. Richoz, Z.K. Tuong, G.S. Bowyer, C.Y.C. Lee, J.R. Ferdinand, E. Gillman, M. McClure, L. Dratva, S.A. Teichmann, et al. 2025. Temporal profiling of human lymphoid tissues reveals coordinated defense against viral challenge. *Nat. Immunol.* 26:215–229. https://doi.org/10.1038/s41590-024-02064-9

Cook, D.N., D.M. Prosser, R. Forster, J. Zhang, N.A. Kuklin, S.J. Abbondanzo, X.D. Niu, S.C. Chen, D.J. Manfra, M.T. Wiekowski, et al. 2000. CCR6 mediates dendritic cell localization, lymphocyte homeostasis, and immune responses in mucosal tissue. *Immunity*. 12:495–503. https://doi.org/10.1016/s1074-7613(00)80201-0

Crotty, S. 2019. T follicular helper cell biology: A decade of discovery and diseases. *Immunity*. 50:1132–1148. https://doi.org/10.1016/j.immuni.2019.04.011

Da Silva, C., C. Wagner, J. Bonnardel, J.-P. Gorvel, and H. Lelouard. 2017. The Peyer's patch mononuclear phagocyte system at steady state and during infection. *Front. Immunol.* 8:1254. https://doi.org/10.3389/fimmu.2017.01254

Davis, S.S. 2001. Nasal vaccines. *Adv. Drug Deliv. Rev.* 51:21–42. https://doi.org/10.1016/s0169-409x(01)00162-4

Denton, A.E., S. Innocentin, E.J. Carr, B.M. Bradford, F. Lafouresse, N.A. Mabbott, U. Mörbe, B. Ludewig, J.R. Groom, K.L. Good-Jacobson, and M.A. Linterman. 2019. Type I interferon induces CXCL13 to support ectopic germinal center formation. *J. Exp. Med.* 216:621–637. https://doi.org/10.1084/jem.20181216

Fritz, J.H., O.L. Rojas, N. Simard, D.D. McCarthy, S. Hapfelmeier, S. Rubino, S.J. Robertson, M. Larijani, J. Gosselin, I.I. Ivanov, et al. 2011. Acquisition of a multifunctional IgA+ plasma cell phenotype in the gut. *Nature*. 481: 199–203. https://doi.org/10.1038/nature10698

Gailleton, R., N.R. Mathew, L. Reusch, K. Schön, L. Scharf, A. Strömberg, A. Cvjetkovic, L. Aziz, J. Hellgren, K.-W. Tang, et al. 2025. Ectopic germinal centers in the nasal turbinates contribute to B cell immunity to intranasal viral infection and vaccination. *Proc. Natl. Acad. Sci. USA*. 122: e2421724122. https://doi.org/10.1073/pnas.2421724122

Gallman, A.E., F.D. Wolfreys, D.N. Nguyen, M. Sandy, Y. Xu, J. An, Z. Li, A. Marson, E. Lu, and J.G. Cyster. 2021. Abcc1 and Ggt5 support lymphocyte guidance through export and catabolism of S-geranylgeranyl-l-glutathione. *Sci. Immunol.* 6:eabg1101. https://doi.org/10.1126/sciimmunol.abg1101

Green, J.A., and J.G. Cyster. 2012. S1PR2 links germinal center confinement and growth regulation. *Immunol. Rev.* 247:36–51. https://doi.org/10.1111/j.1600-065X.2012.01114.x

Haniuda, K., N.M. Edner, Y. Makita, S. Appiah, T.H. Watts, G.F. Wu, T. Dileepan, and J.L. Gommerman. 2025. Mucosal viral infection elicits long-lived IgA responses via type 1 follicular helper T cells. *Cell*. 188: 6774–6790.e21. https://doi.org/10.1016/j.cell.2025.07.022

Hartwell, B.L., M.B. Melo, P. Xiao, A.A. Lemnios, N. Li, J.Y.H. Chang, J. Yu, M.S. Gebre, A. Chang, L. Maiorino, et al. 2022. Intranasal vaccination with lipid-conjugated immunogens promotes antigen transmucosal uptake to drive mucosal and systemic immunity. *Sci. Transl. Med.* 14: eabn1413. https://doi.org/10.1126/scitranslmed.abn1413

Jain, S., M. Bemark, and J. Spencer. 2023. Human gut-associated lymphoid tissue: A dynamic hub propagating modulators of inflammation. *Clin. Transl. Med.* 13:e1417. https://doi.org/10.1002/ctm2.1417

Kelsall, B.L., and W. Strober. 1996. Distinct populations of dendritic cells are present in the subepithelial dome and T cell regions of the murine Peyer's patch. *J. Exp. Med.* 183:237–247. https://doi.org/10.1084/jem.183.1.237

Kimura, S., M. Mutoh, M. Hisamoto, H. Saito, S. Takahashi, T. Asakura, M. Ishii, Y. Nakamura, J. Iida, K. Hase, and T. Iwanaga. 2019. Airway M cells arise in the lower airway due to RANKL signaling and reside in the bronchiolar epithelium associated with iBALT in Murine models of respiratory disease. *Front. Immunol.* 10:1323. https://doi.org/10.3389/fimmu.2019.01323

Kiyono, H., and S. Fukuyama. 2004. NALT- versus Peyer's-patch-mediated mucosal immunity. *Nat. Rev. Immunol.* 4:699–710. https://doi.org/10.1038/nri1439

Komban, R.J., A. Strömberg, A. Biram, J. Cervin, C. Lebrero-Fernández, N. Mabbott, U. Yrlid, Z. Shulman, M. Bemark, and N. Lycke. 2019. Activated Peyer's patch B cells sample antigen directly from M cells in the subepithelial dome. *Nat. Commun.* 10:2423. https://doi.org/10.1038/s41467-019-10144-w

Linehan, J.L., T. Dileepan, S.W. Kashem, D.H. Kaplan, P. Cleary, and M.K. Jenkins. 2015. Generation of Th17 cells in response to intranasal infection requires TGF-β1 from dendritic cells and IL-6 from CD301b+ dendritic cells. *Proc. Natl. Acad. Sci. USA*. 112:12782–12787. https://doi.org/10.1073/pnas.1513532112

Liu, J., and Z. Shulman. 2022. Affinity-based clonal selection in Peyer's patches. *Curr. Opin. Immunol.* 74:100–105. https://doi.org/10.1016/j.coi.2021.11.002

Liu, J., L. Stoler-Barak, H. Hezroni-Bravyi, A. Biram, S. Lebon, N. Davidzohn, M. Kedmi, M. Chemla, D. Pilzer, M. Cohen, et al. 2024. Turbinate-homing IgA-secreting cells originate in the nasal lymphoid tissues. *Nature*. 632:637–646. https://doi.org/10.1038/s41586-024-07729-x

Lund, F.E., and T.D. Randall. 2021. Scent of a vaccine. *Science*. 373:397–399. https://doi.org/10.1126/science.abg9857

Lycke, N.Y., and M. Bemark. 2012. The role of Peyer's patches in synchronizing gut IgA responses. *Front. Immunol.* 3:329. https://doi.org/10.3389/fimmu.2012.00329

Mao, T., B. Israelow, M.A. Peña-Hernández, A. Suberi, L. Zhou, S. Luyten, M. Reschke, H. Dong, R.J. Homer, W.M. Saltzman, and A. Iwasaki. 2022. Unadjuvanted intranasal spike vaccine elicits protective mucosal immunity against sarbecoviruses. *Science*. 378:eabo2523. https://doi.org/10.1126/science.abo2523

Mora, J.R., and U.H. von Andrian. 2008. Differentiation and homing of IgA-secreting cells. *Mucosal Immunol.* 1:96–109. https://doi.org/10.1038/mi.2007.14

Mörbe, U.M., P.B. Jørgensen, T.M. Fenton, N. von Burg, L.B. Riis, J. Spencer, and W.W. Agace. 2021. Human gut-associated lymphoid tissues (GALT); diversity, structure, and function. *Mucosal Immunol.* 14:793–802. https://doi.org/10.1038/s41385-021-00389-4

Moseman, E.A., A.C. Blanchard, D. Nayak, and D.B. McGavern. 2020. T cell engagement of cross-presenting microglia protects the brain from a nasal virus infection. *Sci. Immunol.* 5:eabb1817. https://doi.org/10.1126/sciimmunol.abb1817

Nacer, A., D. Carapau, R. Mitchell, A. Meltzer, A. Shaw, U. Frevert, and E.H. Nardin. 2014. Imaging murine NALT following intranasal immunization with flagellin-modified circumsporozoite protein malaria vaccines. *Mucosal Immunol.* 7:304–314. https://doi.org/10.1038/mi.2013.48

Nakashima, T., and Y. Hamashima. 1980. Local immune system of nasal mucosa in inflammation. IgA distribution and secretory activity. *Ann. Otol Rhinol Laryngol.* 89:140–146. https://doi.org/10.1177/000348948008900210

Neutra, M.R., A. Frey, and J.P. Kraehenbuhl. 1996. Epithelial M cells: Gateways for mucosal infection and immunization. *Cell*. 86:345–348. https://doi.org/10.1016/s0092-8674(00)80106-3

Nowosad, C.R., L. Mesin, T.B.R. Castro, C. Wichmann, G.P. Donaldson, T. Araki, A. Schiepers, A.A.K. Lockhart, A.M. Bilate, D. Mucida, and G.D. Victora. 2020. Tunable dynamics of B cell selection in gut germinal centres. *Nature*. 588:321–326. https://doi.org/10.1038/s41586-020-2865-9

Oh, J.E., E. Song, M. Moriyama, P. Wong, S. Zhang, R. Jiang, S. Strohmeier, S.H. Kleinstein, F. Krammer, and A. Iwasaki. 2021. Intranasal priming induces local lung-resident B cell populations that secrete protective mucosal antiviral IgA. *Sci. Immunol.* 6:eabj5129. https://doi.org/10.1126/sciimmunol.abj5129

Okada, H., M. Tsuda, N. Kojima, H. Watanabe, G. Harata, K. Miyazawa, D. Kyoui, S. Hachimura, Y. Takahashi, K. Takahashi, and A. Hosono. 2025. The constitutive presence of commensal bacteria contributes to the abundance of cecal IgG2b+ B cells and the supply of serum IgG2b reactive to commensal bacteria in adult mice. *Biosci. Microbiota Food Health*. 44: 128–136. https://doi.org/10.12938/bmfh.2024-083

Pabst, O., and C.R. Nowosad. 2023. B cells and the intestinal microbiome in time, space and place. *Semin. Immunol.* 69:101806. https://doi.org/10.1016/j.smim.2023.101806

Pabst, O., and E. Slack. 2020. IgA and the intestinal microbiota: The importance of being specific. *Mucosal Immunol.* 13:12–21. https://doi.org/10.1038/s41385-019-0227-4

Pereira, J.P., L.M. Kelly, Y. Xu, and J.G. Cyster. 2009. EBI2 mediates B cell segregation between the outer and centre follicle. *Nature*. 460:1122–1126. https://doi.org/10.1038/nature08226

Pizzolla, A., Z. Wang, J.R. Groom, K. Kedzierska, A.G. Brooks, P.C. Reading, and L.M. Wakim. 2017. Nasal-associated lymphoid tissues (NALTs) support the recall but not priming of influenza virus-specific cytotoxic T cells. *Proc. Natl. Acad. Sci. USA*. 114:5225–5230. https://doi.org/10.1073/pnas.1620194114

Ramirez, S.I., F. Faraji, L.B. Hills, P.G. Lopez, B. Goodwin, H.D. Stacey, H.J. Sutton, K.M. Hastie, E.O. Saphire, H.J. Kim, et al. 2024. Immunological memory diversity in the human upper airway. *Nature*. 632:630–636. https://doi.org/10.1038/s41586-024-07748-8

Randall, T.D. 2015. Structure, organization, and development of the mucosal immune system of the respiratory tract. *Mucosal Immunol.* 1:43–61. https://doi.org/10.1016/B978-0-12-415847-4.00004-5

Reboldi, A., T.I. Arnon, L.B. Rodda, A. Atakilit, D. Sheppard, and J.G. Cyster. 2016. IgA production requires B cell interaction with subepithelial dendritic cells in Peyer's patches. *Science*. 352:aaf4822. https://doi.org/10.1126/science.aaf4822

Reboldi, A., and J.G. Cyster. 2016. Peyer's patches: Organizing B-cell responses at the intestinal frontier. *Immunol. Rev.* 271:230–245. https://doi.org/10.1111/imr.12400

Reboldi, A., E.V. Dang, J.G. McDonald, G. Liang, D.W. Russell, and J.G. Cyster. 2014. Inflammation. 25-Hydroxycholesterol suppresses interleukin-1-driven inflammation downstream of type I interferon. *Science* 345: 679–684. https://doi.org/10.1126/science.1254790

Reimer, D., A.Y.S. Lee, J. Bannan, P. Fromm, E.E. Kara, I. Comerford, S. McColl, F. Wiede, D. Mielenz, and H. Körner. 2017. Early CCR6 expression on B cells modulates germinal centre kinetics and efficient antibody responses. *Immunol. Cell Biol.* 95:33–41. https://doi.org/10.1038/icb.2016.68

Riedel, R., R. Addo, M. Ferreira-Gomes, G.A. Heinz, F. Heinrich, J. Kummer, V. Greiff, D. Schulz, C. Klaeden, R. Cornelis, et al. 2020. Discrete populations of isotype-switched memory B lymphocytes are maintained in murine spleen and bone marrow. *Nat. Commun.* 11:2570. https://doi.org/10.1038/s41467-020-16464-6

Rommel, P.C., D. Bosque, A.D. Gitlin, G.F. Croft, N. Heintz, R. Casellas, M.C. Nussenzweig, S. Kriaucionis, and D.F. Robbiani. 2013. Fate mapping for activation-induced cytidine deaminase (AID) marks non-lymphoid cells during mouse development. *PLoS One*. 8:e69208. https://doi.org/10.1371/journal.pone.0069208

Schulz, O., and O. Pabst. 2013. Antigen sampling in the small intestine. *Trends Immunol.* 34:155–161. https://doi.org/10.1016/j.it.2012.09.006

Schwickert, T.A., B. Alabyev, T. Manser, and M.C. Nussenzweig. 2009. Germinal center reutilization by newly activated B cells. *J. Exp. Med.* 206: 2907–2914. https://doi.org/10.1084/jem.20091225

Schwickert, T.A., G.D. Victora, D.R. Fooksman, A.O. Kamphorst, M.R. Mugnier, A.D. Gitlin, M.L. Dustin, and M.C. Nussenzweig. 2011. A dynamic T cell-limited checkpoint regulates affinity-dependent B cell entry into the germinal center. *J. Exp. Med.* 208:1243–1252. https://doi.org/10.1084/jem.20102477

Shulman, Z., A.D. Gitlin, J.S. Weinstein, B. Lainez, E. Esplugues, R.A. Flavell, J.E. Craft, and M.C. Nussenzweig. 2014. Dynamic signaling by T follicular helper cells during germinal center B cell selection. *Science*. 345: 1058–1062. https://doi.org/10.1126/science.1257861

Siniscalco, E.R., H. Meng, G. Gabernet, G.A. Pacheco, S. Saghaei, S.I. Ramirez, L.B. Hills, F. Faraji, S. Chen, X. Yin, et al. 2025. Sequential class switching generates antigen-specific gut IgA from IgG1 B cells. *Immunity*. 58:3075–3093.e6. https://doi.org/10.1016/j.immuni.2025.10.022

Siniscalco, E.R., A. Williams, and S.C. Eisenbarth. 2024. All roads lead to IgA: Mapping the many pathways of IgA induction in the gut. *Immunol. Rev.* 326:66–82. https://doi.org/10.1111/imr.13369

Topol, E.J., and A. Iwasaki. 2022. Operation nasal vaccine—Lightning speed to counter COVID-19. *Sci. Immunol.* 7:eadd9947. https://doi.org/10.1126/sciimmunol.add9947

Tsuda, M., H. Okada, N. Kojima, F. Ishihama, Y. Muraki, T. Oguma, N. Hattori, T. Mizoguchi, K. Mori, S. Hachimura, et al. 2022. Cecal patches generate abundant IgG2b-bearing B cells that are reactive to commensal microbiota. *J. Immunol. Res.* 2022:3974141. https://doi.org/10.1155/2022/3974141

Ualiyeva, S., E. Lemire, C. Wong, A. Perniss, A.A. Boyd, E.C. Avilés, D.G. Minichetti, A. Maxfield, R. Roditi, I. Matsumoto, et al. 2024. A nasal cell atlas reveals heterogeneity of tuft cells and their role in directing olfactory stem cell proliferation. *Sci. Immunol.* 9:eabq4341. https://doi.org/10.1126/sciimmunol.abq4341

Wellford, S.A., A.P. Moseman, K. Dao, K.E. Wright, A. Chen, J.E. Plevin, T.-C. Liao, N. Mehta, and E.A. Moseman. 2022. Mucosal plasma cells are required to protect the upper airway and brain from infection. *Immunity*. 55:2118–2134.e6. https://doi.org/10.1016/j.immuni.2022.08.017

Yang Shih, T.-A., E. Meffre, M. Roederer, and M.C. Nussenzweig. 2002. Role of BCR affinity in T cell–dependent antibody responses in vivo. *Nat. Immunol.* 3:570–575. https://doi.org/10.1038/ni803

Supplemental material

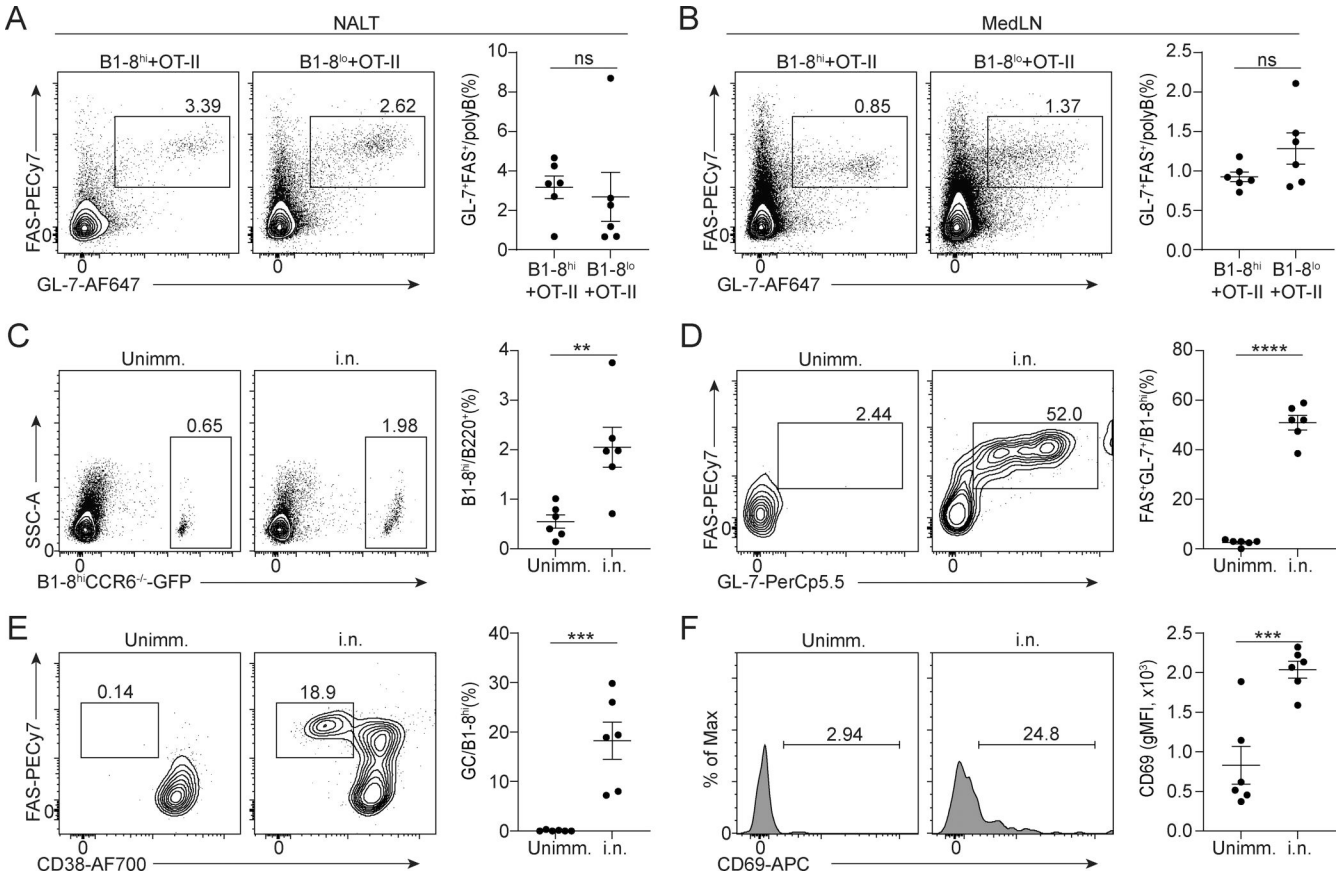

Figure S1. **Polyclonal immune responses and the activation and expansion of CCR6-deficient B1-8hi B cells in the NALT. (A and B)** Flow cytometry plots and GC percentage of polyclonal B cells in the NALT and MedLN of mice that received B1-8^{hi} or B1-8^{lo} B cells and OT-II T cells, followed by nasal vaccination with NP-OVA + MPLA. The data are from the experiments of Fig. 1, C and D; and Fig. 3, A–F. GL7$^+$ FAS$^+$ populations were gated from non–B1-8 B220$^+$ B cells. *n* = 6; two independent experiments. Unpaired two-tailed Student's *t* test; data represent mean ± SEM; ns, not significant. **(C–F)** Flow cytometry analysis of CCR6$^{-/-}$ B1-8^{hi} B cells in the NALT of unimmunized mice and after nasal vaccination. WT mice were adoptively transferred with GFP$^+$ CCR6$^{-/-}$ B1-8^{hi} B cells and CD45.1$^+$ OT-II T cells, followed by i.n. NP-OVA + MPLA, or were left unimmunized. NALTs were collected and analyzed by flow cytometry on day 5 after i.n. NP-OVA + MPLA immunization. CCR6$^{-/-}$ GFP$^+$ B1-8^{hi} B cells gated from B220$^+$ population (C); activated (FAS$^+$, GL-7$^+$) (D), GC (FAS$^+$, CD38$^-$) (E), and CD69$^+$ B cell (F) subsets are gated from CCR6$^{-/-}$ GFP$^+$ B1-8^{hi} B220$^+$ cells. *n* = 6; two independent experiments. Unpaired two-tailed Student's *t* test; Data represent mean ± SEM; **, P < 0.01; ***, P < 0.001; ****, P < 0.0001.